Lime pastes with different kneading water: pore structure and capillary porosity

M. Arandigoyen[a], J.L Pérez Bernal[b], M.A Bello López[b], J.I. Alvarez [a,*]

[a] *Departamento de Química, Universidad de Navarra, 31080 Pamplona, Spain*

[b] *Departamento de Química Analítica, Universidad de Sevilla, Apdo. 1065, 41080 Sevilla, Spain*

Nº of pages: 34

Nº of tables: 4

Nº of figures: 13

PACS Codes: 81.05.Rm 68.35.Fx

Keywords: Lime pastes, porosimetry, fractal geometry, capillary, kneading water, microstructure

Please, send all correspondence to:

Dr. José I. Alvarez Galindo
Dpto. de Química
Fac. de Ciencias
Universidad de Navarra
C/ Irunlarrea s/n
31.080 Pamplona (Navarra)
Spain
Phone: 34 948 425600
Fax: 34 948 425649
E-mail: jalvarez@unav.es

Lime pastes with different kneading water: pore structure and capillary porosity

M. Arandigoyen[a], J.L Pérez Bernal[b], M.A Bello López[b], J.I. Alvarez [a,*]

[a] *Departamento de Química, Universidad de Navarra, 31080 Pamplona, Spain*

[b] *Departamento de Química Analítica, Universidad de Sevilla, Apdo. 1065, 41080 Sevilla, Spain*

ABSTRACT:

Lime mortars to be used in restoration works of Cultural Heritage are being more and more studied. The knowledge on the lime pastes allows to understand the behaviour of the binder fraction. The aim of this work is to study the influence of the kneading water on two critical aspects of the lime-pastes: pore structure and capillary porosity, because both of them are related to the service life of the material, particularly with the moisture transport. Mercury intrusion porosimetry has been performed to establish the pore size distribution: one pore range has been checked in the different pastes tested, setting linear relationships between the pore diameter and the water/lime ratio.

Fractal geometry has been used from the MIP results in order to evaluate the pore surface complexity, as a function of the kneading water. From the results, it can be concluded that kneading water is only responsible for a swelling of the structure, but it does not change the pore surface (keeping constant the surface fractal dimension). DIA analysis has been carried out, confirming the previous results. Finally, the correlation obtained between the capillary coefficient and the water/lime ratio confirms the postulated pore structure for the different amount of kneading water in lime-pastes.

PACS Codes: 81.05.Rm 68.35.Fx

Keywords: Lime pastes, porosimetry, fractal geometry, capillary, kneading water, microstructure

1. Introduction

The amount of kneading water, defining as water-binder ratio, has been established as one of the most important parameters in the binding pastes obtaining. Actually, the original water content in the mixture regulates the rate of strength development and the ultimate strength of the paste [1].

Capillary porosity is formed from residual spaces occupied by original kneading water. In several works the capillary process is used as indicative of the future degradation of buildings materials [2-5]. The capillary transport is the main driving mechanism for the chloride and the sulphate ions, and absorbed water by capillarity can be a problem as consequence of the freezing/thawing cycles. The capillary behaviour is a consequence of the porous nature of building materials and their exposition to the environmental conditions.

When a capillary is in contact with a liquid, it creates a difference of pressure ΔP reversely proportional to its radius, forcing the liquid to go inside the capillary, as shows Equation 1:

$$\Delta P = 2\gamma \cos\theta / r \qquad \text{(Eq. 1)}$$

where γ is the surface tension of the liquid, θ the contact angle and r the radius of the capillary. The parallel tube model of porous media has been extensively reported [4], as shows Equation 2, which considers the material as a group of straight parallel capillaries along of this, instead of a random porous material:

$$M_S = C_A \cdot \sqrt{t} + C_0 \qquad \text{(Eq. 2)}$$

where M_S is the mass of water absorbed by unity of surface (g/m^2), C_A is the capillarity coefficient ($g/m^2 \cdot s^{-1/2}$), t the time (s) and C_0 a value function of the surface of contact with the water (g/m^2). Equation 2 surges as consequence of applying the Darcy's law to a capillary tube.

As a consequence, this capillary porosity as well as the pore structure of the binding materials, plays an important role in moisture transport, related with durability, degradation and service life of the building materials [4,6].

Fractal geometry has been widely used for different studies on porous solids, i.e. concrete, porous silicas, colloidal clay aggregates [7]. Mercury intrusion porosimetry data can be used to calculate the pore surface fractal dimension, a descriptor of the paste pore surface [8].

In the framework of this research, lime-based mortars are studied in order to be used in restoration works of Cultural Heritage [9,10]. Due to the fact that the paste is the main factor of porosity in a binding material [5], in this paper lime pastes were considered.

The aim of this work is to evaluate the pore structure in carbonated lime pastes prepared with different kneading water, using the fractal geometry, and also the capillary sorption as a relevant hygrometric property.

2. Experimental work

2.1. Pastes preparation

A hydrated commercial lime powder (Ecobat®) (supplied by Calinsa S.A, Navarra, of the class CL90 according to Spanish standard [11]) was used. Chemical and mineralogical composition of this aerial lime is discussed in section 3.1 below.

60 cylindrical specimens of 4 cm (diameter of 3.4 cm) were elaborated blending this lime with different amounts of kneading water in order to obtain six different W/L (water/lime) ratios (0.8, 0.9, 1.0, 1.1, 1.2 and 1.3), with 10 specimens in each group. The best workability has been obtained for 0.9 and 1.0 W/L ratio pastes, broading the study to W/L ratios below and above these values.

The pastes were blended for 5 minutes in a Proeti ETI 26.0072 mixer, molded in the cylindrical casts and demolded 3 days later. The specimens were cured in a vertical position in ambient laboratory conditions (RH 60 ± 10% and 20 ± 5ºC) for 2 years, with the aim of to achieve an almost complete lime carbonation. The surrounding CO_2 in the room was estimated to be the standard atmospheric concentration (0.033 ± 0.001% by volume).

XRD and TG-DTA studies were carried out at different times in order to evaluate the carbonation degree. In order to evaluate the properties of the pastes, the specimens were dried until 90ºC in a progressive heating with the purpose to avoid damages because of cracking in the material. Thus, the water was totally removed from all the specimens.

All reported analytical results are the average value of the three identical specimens tested.

2.2. Analytical methodology

2.2.1. XRD analysis

The mineralogical phases present in the specimens were determined by means of X-ray diffraction (XRD) using a Brucker D8 Advance diffractometer, according to the diffraction powder method, with a $CuK_{\alpha 1}$ radiation and 0.02 2θ increment and 1 $s \cdot step^{-1}$, sweep from 2 to 90º 2θ. The results were compared with the ICDD database.

2.2.2. Thermal analysis

Differential thermal and thermogravimetric analysis (DTA-TG) were conducted using a simultaneous TGA-sDTA 851 Mettler Toledo thermoanalyser, with alumina crucibles, fitted with holed lids, at a 10ºC·min^{-1} heating rate, under static air atmosphere.

2.2.3. SEM and DIA analyses

Scanning electron microscopy (SEM) in a Digital Scanning Microscope DSM-940 A Zeiss was used for microscopic observation of the morphology of the microstructure. Moreover, representative samples were submitted to scanning electron microscopy in order to perform digital image analysis (DIA). Samples for microscopy were prepared by low viscosity epoxy resin impregnation [12] at vacuum, followed by grounding and polishing [13,14]. Prior to embedding, samples were dried for 48 hours at 50ºC. Software Imagen J 1.32J was used to obtain segmented images and pore characteristics of the samples.

2.2.4. Pore structure

The pore structure was evaluated in two ways:

2.2.4.1. Open porosity measurement: the total porosity is expressed as P, in percent, and is determined according to the water saturation test [15] with a hydrostatics balance.

2.2.4.2. Pore size distribution is evaluated using the mercury intrusion porosimetry technique with a Micrometrics 9320 Poresizer mercury porosimeter,

with automatically registers pressure, pore diameter, intrusion volume and pore surface area.

2.2.5. Capillary absorption

The capillary water absorption was measured with the assembly presented in Fig. 1. The specimen is holding from the balance. Water only gets in touch with the specimen by the bottom face. At this moment, the electronic timekeeping starts and the water is coming in the specimen by capillarity. The weight increase due to the retained water is stored by the balance and the computer. Owing to the small size of the specimen, the amount of retained water is small enough to neglect any change in the water level, so it remains constant. Test was carried out during several hours, with the aim to achieve a complete saturation of the specimen.

3. Results and discussion

3.1. Mineralogical and chemical composition of the pastes

Table 1 presents the chemical analysis of the lime used. XRD and TG-DTA analyses were performed in order to study the mineralogical composition of the lime. Results show that only two mineralogical phases are present: portlandite ($Ca(OH)_2$) (ICDD 44-1481) as the main phase, and calcite ($CaCO_3$) (ICDD 05-0586), as a result of a slight carbonation (Fig.2) [9]. TG-DTA study confirms those results (Fig.3): a weight loss at around 450ºC can be attributed to the $Ca(OH)_2$ dehydroxilation, whereas the weight loss at ~750ºC is due to the $CaCO_3$ decarbonation [16]. The quantification of the TG curve gives 87% of $Ca(OH)_2$, 10% of $CaCO_3$ and 3% of humidity. No magnesium compounds (MgO, $Mg(OH)_2$, dolomite or magnesite) were checked.

As described by Rodríguez Navarro et al. [17], carbonation of a lime-mortar takes place when CO_2 dissolves in water and reacts with dissolved calcium hydroxide. This reaction results in a calcium carbonate precipitation, due to the rapid supersaturation with respect to $CaCO_3$ in the solution existing in the mortar pores (which contains dissolved CO_2 and $Ca(OH)_2$ in the condensed water) [18].

The presence of water is essential for the carbonation process, as it has been confirmed by previous research [9,19]. Therefore, the kneading water acquires a great importance in the carbonation of lime. This water can be retained by capillary, adsorbed and condensed in the surface of the pores.

XRD and TG-DTA studies were carried out at different times in order to evaluate the carbonation degree. XRD showed a negligible amount of $Ca(OH)_2$ after one curing year [9]. After two curing years any diffraction peak of $Ca(OH)_2$ has not been checked. TG results confirm the XRD study: no dehydroxilation step of $Ca(OH)_2$ (~ 480ºC) can be reported. Only the weight loss between 700-850ºC can be observed. This loss is related to $CaCO_3$ decarbonation. Due to the similarity between all the results, Figs. 4 and 5 show as an example XRD and TG-DTA curves of a sample (W/L=0.8) after two curing years. For these studies, sample was taken from the core of the specimen (the most inaccessible place for surrounding CO_2). Result allow to establish a complete and identical (between the external part and the core of the samples) carbonation.

3.2. SEM observations

Given that calcite crystals replace portlandite crystals, and commercial nonaged hydrated lime mortars carbonates as a closer-to-equilibrium diffusion limited system [18], microstructure of these carbonated lime-pastes must be uncomplicated. In fact, the precipitate of calcium carbonate as calcite or one of its polymorphic forms allows to an

accumulation of crystals, very close as a consequence of the reported solid volume increase when portlandite transforms to calcite (11.8%) [18].

SEM micrographs obtained from the carbonated lime-pastes show their microstructure at different magnifications (Fig. 6).

As it is proved, calcite crystals have irregular polyhedral shapes, so the internal surface of the pores could be expected having irregular structure. Microstructure of these pastes is not complex: several aggregates of small crystals as well as the pores can be observed. No great differences between the samples have been obtained. Fig. 7 shows other SEM micrographs obtained to DIA analysis: it can be observed very small differences between the different W/L ratio samples. Perhaps, samples with higher W/L ratio show larger aggregates of calcite crystals, and the pores are larger than in samples with lower W/L ratio. However, the general microstructure appears to be very similar, as expected, due to the same mineralogical composition of the samples.

3.3. Pore structure

3.3.1. Open Porosity

Due to the previously discussed SEM observations, carbonated lime-pastes could be described as two different phases: calcite crystals and the void between crystals (i.e. the pore system).

The evaporation of the excess of kneading water from residual spaces previously occupied leads the pores into the structure [1]. Increased kneading water in the original paste must allow to an increased porosity.

Table 2 shows the experimental values of the residual spaces. The open porosity has been determined from the result of the MIP technique (P(Hg)) and from the absorption of water by immersion, with a hydrostatics balance (P(W)).

Results are coherent, showing a porosity increment related to a kneading water rise, as expected.

In both techniques the results are quite similar; nowadays the porosities obtained with the MIP technique are a bit higher in all the cases than with the water immersion technique. This fact can be attributed to the different procedure. MIP gives a higher porosity due to the mercury injection by using pressure, so this technique can reach smaller pores than water immersion technique. With the water immersion technique, the accuracy is good with small standard deviations.

All the specimens have porosity higher than 50%, increasing with the amount of kneading water employed until almost 65% of porosity. As previously reported [9], larger amount of binder cause porosity increase. In the pastes of the current work, open porosities are twice as much as porosities of lime mortars [9]. This fact can be explained due to the absence of any aggregate (with low porosity) in lime pastes.

3.3.2. Pore size distribution

A pore size distribution analysis has been carried out in a wide range from 350μm to 0.003μm pore diameter. However, lime pastes show porosity in a narrow range of pores [9], except some possible air burbles that could be included during the preparation [20].

Fig. 8 shows the results of the pore size distribution from MIP for the six different W/L pastes. The accuracy of the measurement has been good, even though the possible air burbles. In agreement with a previous work on lime-based mortars [9], it can see that all

the pores are smaller than 2μm, and there is a main diameter of pore between 0.5 and 1μm, which increases when W/L rises.

Fig. 9 presents the values of the main pore diameter as well as the threshold diameter versus W/L ratio. Threshold diameter has been defined as a diameter corresponding to a pressure below which very little intrusion into the specimen is recorded, and immediately above which the greatest portion of the intrusion takes place. The threshold diameter is characteristic of each porous material [21].

Both of them, the main and threshold diameters, increase when higher amount of kneading water was used during paste preparation. From the equations of Fig. 9, it can be established the highest difference $D_{threshold} - D_{main}$ for the highest W/L ratio. As a consequence the range of pores with different diameter (between $D_{threshold}$ and D_{main} values) increases in this pore structure. This result is consistent with the highest kneading water amount and its evaporation later. For the lime used, linear relationships have been clearly established between the kneading water during the paste preparation and the D_{main} and the $D_{threshold}$ in the carbonated specimen.

From these results, it can be seen that the kneading water increase allows to a similar pore structure, with higher D_{main} and a wider range of pores between D_{main} and $D_{threshold}$. However, no changes on the small pores or other pore characteristics can be determined. Therefore, it can put forward that the solid phase (calcite crystals) remains almost unchanged when W/L ratio increases, swelling the pore structure, as Fig. 10 simulates.

In order to confirm these results, SEM images were segmented and submitted to DIA in order to establish the porosity, mean pore size and pore shape (Fig. 7) (Table 3). The segmented images show an agreement with the simulated pore structure: W/L ratio increase lead to a swelling in the pore structure. The values of the porosity obtained by DIA (through the porous area fraction) (Table 3) agree with the porosity values (MIP

water immersion), increasing when W/L rises. The mean Feret diameter also shows an increase, and this fact confirms the D_{main} evolution obtained by MIP. Finally, the mean circularity (giving an idea on the pore shape) appears to be very similar in all the studies samples, confirming the previous assumption.

3.3.3. Surface fractal dimension

In a previous work [22], pore fractal objects were defined as dense objects within exist a distribution of pores with a fractal structure. Fractal geometry is used to describe chaotic systems which are characterized by their invariability at any scale used to examine them: any part or the system looks the same as the whole (self-similarity) [7]. System is determined by fractal dimension value, which is defined as an intermediate dimension between the Euclidean dimensions (point 0, line 1, plane 2 and volume 3) as a consequence of the complexity of the system [23].

In these lime pastes the surface fractal dimension (D_S) (i.e. the Koch surface) is studied, taking values between 2 (plane) and 3 (volume). This value (D_S) gives a description of the heterogeneity and complexity of the system. In a previous paper, several methods to calculate this parameter were explained and compared [7]. In this case a model elaborated by Zhang and Li [24] derived from thermodynamic considerations and dimensional analysis has been applied to the mercury intrusion porosimetry data, obtaining good correlation coefficients. Zhang and Li model is applied to the porosimeter data (Equation 3), and the D_S is obtained for each paste:

$$Q_n = -\sum_{i=1}^{n} \overline{P}_i \Delta V_i \propto r_n^{2-D} V_n^{D/3} = W_n \qquad \text{(Eq. 3)}$$

where P is the pressure applied, V the volume of intruded mercury, r the pore radius and D the surface fractal dimension. This model seems to adjust in a good way to this kind of materials, as proved by the correlation coefficients higher than 0.99. The study has been realized in the interval between 0.021μm and 1.0μm. According to Pfeifer and Obert [25], to accept an experimental fractal dimension, the pore diameter range used to calculate the fractal dimension should expand one decade or more. This requirement has been fulfilled in the present work.

From these results (Table 4), the values of D_S obtained by MIP remain almost unchanged with the amount of kneading water used in the preparation of the pastes. The slight variation in the values can be attributed to the small differences in the pore interval used (from the 0.021μm to the maximum close to 1.0μm). This D_S invariability shows an opposite behaviour with respect to water/binder ratio in cement materials, in which a change is reported due to the complexity of their structure [26].

The constant value of D_S in lime pastes with different W/L ratio confirms the MIP results, discussed in the previous section. Thus, in lime pastes the amount of kneading water establishes the distance between solid particles in the conglomerate of calcite crystals. This kneading water is responsible for the swelling degree of the structure, but it leaves unvarying the complexity of the pore surface, as proved by D_S values.

Table 4 also shows the DIA fractal calculations. As can be seen fractal dimension is nearly the same for all samples, confirming the tendency obtained by MIP. DIA obtained values are lower than MIP values: this fact can be due to the different underlying measuring procedure. While fractal dimension in MIP measures arises from the pore size distribution in DIA fractality is due to the pore shape.

The similarity of fractal dimension obtained by DIA calculations could be adscribed to the similarity of the pore structures for the studied samples.

3.4. Capillary absorption

Martys and Ferraris [4] described in a previous research the capillary transport in mortars and concrete. These materials, with cement paste as binding phase, present at early times the behaviour of typical capillary sorption theories: the total water uptaken increased with the $t^{1/2}$. However, at longer times, the sorption behaviour has been proved to be different.

Fig. 11 presents the mass of water absorbed by unity of surface versus time. An increase is observed, up to the saturation value. It could be expressed versus $t^{1/2}$, in order to obtain linear relationships. The calculated slopes of these straight lines give the C_A values, i.e. the capillary coefficients (g/cm^2s), according to Eq. 2.

As can be observed, the capillary sorption behaviour matches the typically reported, even at longer test times.

In order to compare the different capillary coefficients obtained for the lime pastes with different kneading water, Fig. 12 shows the capillary coefficient represented vs. the W/L ratio.

As can be observed, capillary coefficient linearly increases with the W/L ratio, showing a good correlation factor (R^2 = 0.9958) for the experimental equation. Within the experimental range, the capillary coefficient in carbonated pastes can be predictable as a function of the W/L ratio.

According to the pore structure discussed in the previous section, the pore size distribution of these lime pastes shows only one size of pores, which have irregular shape (defined by the same D_S surface fractal dimension). The main diameter of these pores increases when W/L ratio rises.

Owing to the fact that the capillary sorptivity force (as a pressure difference) increases when the pore diameter drops [4], the capillary coefficient was expected to be higher for pastes with a smaller pore diameter at the same porosity. The experimental results can be explained due to the previously reported higher porosity for higher W/L ratio pastes, so pastes with higher W/L ratio uptake more water owing to their higher amount of pores, as Fig. 13 presents.

In binding materials, sorptivity has been reported as the main controlling factor determining the service life [2,4]. Lime pastes prepared with high amount of kneading water, due to their proved high capillary absorption, could provide a rapid means of ingress of moisture and soluble salts.

Conclusions

1) Porosity of carbonated lime pastes shows an expected increases when W/L ratio used in the paste preparation increases. The pore structure evaluated by MIP has determined one pore range, with higher pore diameter at higher amount of kneading water. This fact has been confirmed by DIA. Linear relationships have been established between the main pore diameter and the threshold diameter with the W/L ratio.

2) By means of the fractal geometry, a constant value of the D_S has been determined for all pastes. This fact allows to prove that kneading water remains unvarying the pore surface, only responsible for a swelling of the structure (increasing the pore diameter).

3) A good linear correlation has been calculated between the capillary coefficient and the W/L ratio, allowing to predict the capillary absorption of the water in carbonated lime pastes. Results of the capillary sorptivity agree with the postulated pore structure: pastes with higher W/L ratio uptake more water amount, and this can be a way of deterioration of material.

Acknowledgements

The present study was supported by the Spanish Ministerio de Ciencia y Tecnología, Plan Nacional de Investigación, Desarrollo e Innovación Tecnológica (I+D+I) program, Project MAT 2000-1347.

References

[1] S. Sahu, S. Badger, N. Thaulow, R.J. Lee, Cem. Concr. Comp. 26 (2004) 987-992.

[2] A. Benazzouk, O. Douzane, M. Quéneudec, Cem. Concr. Comp. 26 (2004) 21-29.

[3] L. Basheer, J. Kropp, D.J. Cleland, Constr. Build. Mater. 15 (2001) 93-103.

[4] N.S. Martys, C.F. Ferraris, Cem. Concr. Res. 27 (5) (1997) 747-760.

[5] S. Kolias, C. Georgiou, Cem. Concr. Comp 27 (2005) 211-216.

[6] M.S. Goual, F. de Barquin, M.L. Benmaled, A. Bali, M. Quéneudec, Cem. Concr. Res. 30 (2000) 1559-1563.

[7] J.L. Pérez Bernal, M.A Bello López, Appl. Surf. Sci. 185 (2001) 99-107.

[8] J.L. Pérez Bernal, M.A. Bello López, Appl. Surf. Sci. 161 (2000) 47-53.

[9] J. Lanas, J.I. Alvarez, Cem. Concr. Res. 33 (2003) 1867-1876.

[10] J. Lanas, J.L. Pérez Bernal, M.A. Bello, J.I Alvarez, Cem. Concr. Res. 34 (2004) 2191-2201.

[11] UNE-EN 459-1, Building Lime: Part 1. Definition, specification and conformity criteria, 1996.

[12] D.A. Lange, H.M. Jennings, S.P. Shah, Cem. Concr. Res. 24(5) (1994) 841-853.

[13] P.E. Stutzman, J.R. Clifton, in Proceedings from Twenty-First International Conference on Cement Microscopy (1999) 10-22.

[14] P.E. Sutzman, Cem. Concr. Comp. 26 (2004) 957-966.

[15] RILEM, Mater. Struct. 13 (1980) 175-253.

[16] T.L. Webb, J.E. Krüger, Carbonates, In: R.C. McKenzie (Ed.), Differential Thermal Analysis, Academic Press, London, 1970, pp. 238-266.

[17] C. Rodríguez Navarro, O. Cazalla, K. Elert, E. Sebastián, JSTOR Series A 458 (2002) 2261-2273.

[18] O. Cazalla, C. Rodríguez-Navarro, E. Sebastián, G. Cultrone, J. Am. Ceram. Soc. 83 (2000) 1070-1076.

[19] D.R. Moorehead, Cem. Concr. Res. 16 (1986) 700-708.

[20] K.K. Aligazaki, P.D. Cady, Cem. Concr. Res. 29 (2) (1999) 273-280.

[21] S. Diamond. Cem. Concr. Res. 29 (1999) 1181 – 1188.

[22] Y. Wang, S. Diamond, Cem. Concr. Res. 31 (2001) 1385-1392.

[23] A. Stazi, M. D'Orazio, E.Quagliarini, Build. Environ 37 (2002) 733-739.

[24] B. Zhang, S Li, Ind. Eng. Chem. Res. 34 (1995) 1383-1386.

[25] P. Pfeifer, M. Obert, in: D. Avnir (Ed.), The Fractal Approach to Heterogeneous Chemistry, Wiley, New York, 1989, p.16.

[26] X. Ji, S.Y.N Chan, N. Feng, Cem. Concr. Res. 27 (1997) 1691-1699.

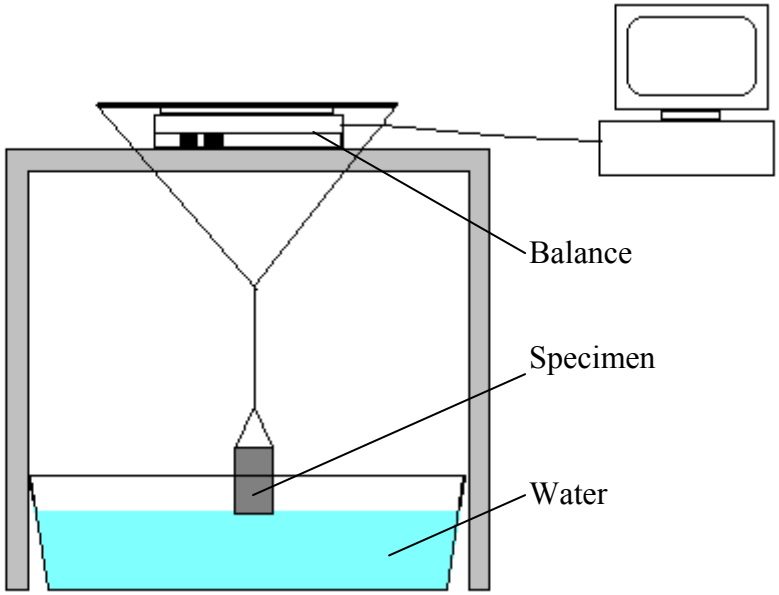

Figure 1. Diagram of the assembly used to the capillary sorption measurements.

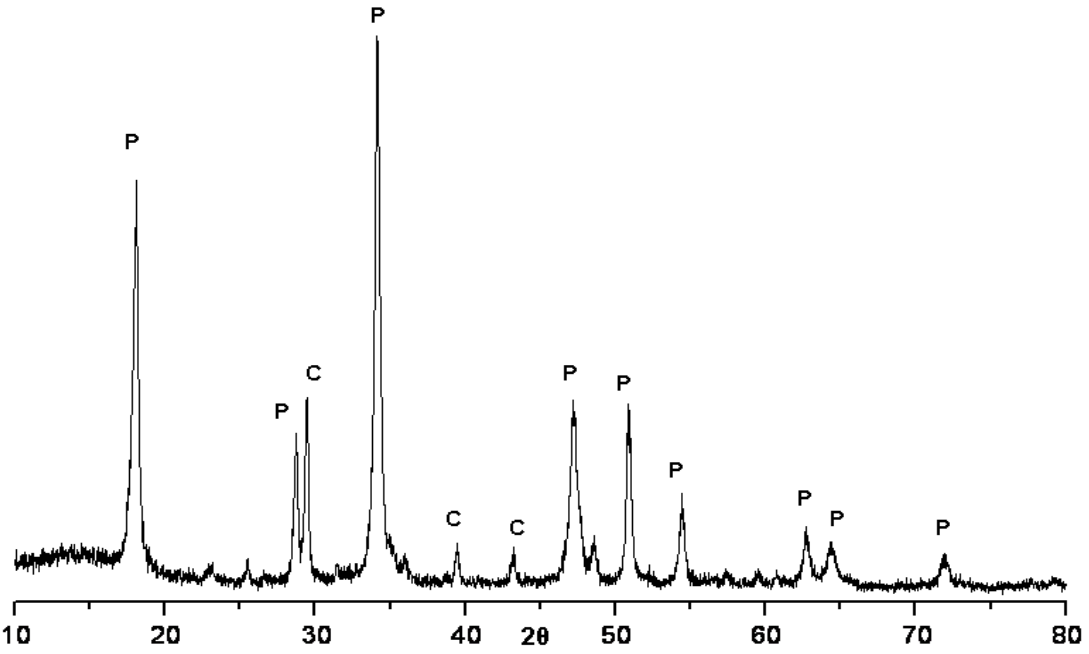

Figure 2. XRD of the lime Ecobat® (C: Calcite (ICDD 05-0586); P: Portlandite (ICDD 44-1481)).

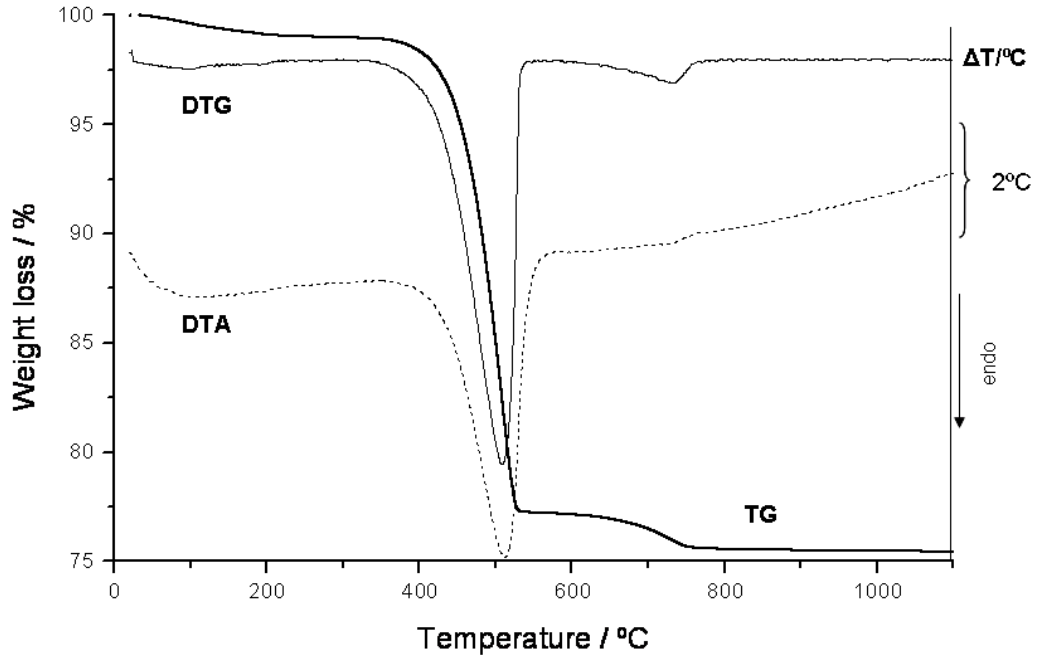

Figure 3. TG, DTG and DTA curves of the lime Ecobat®.

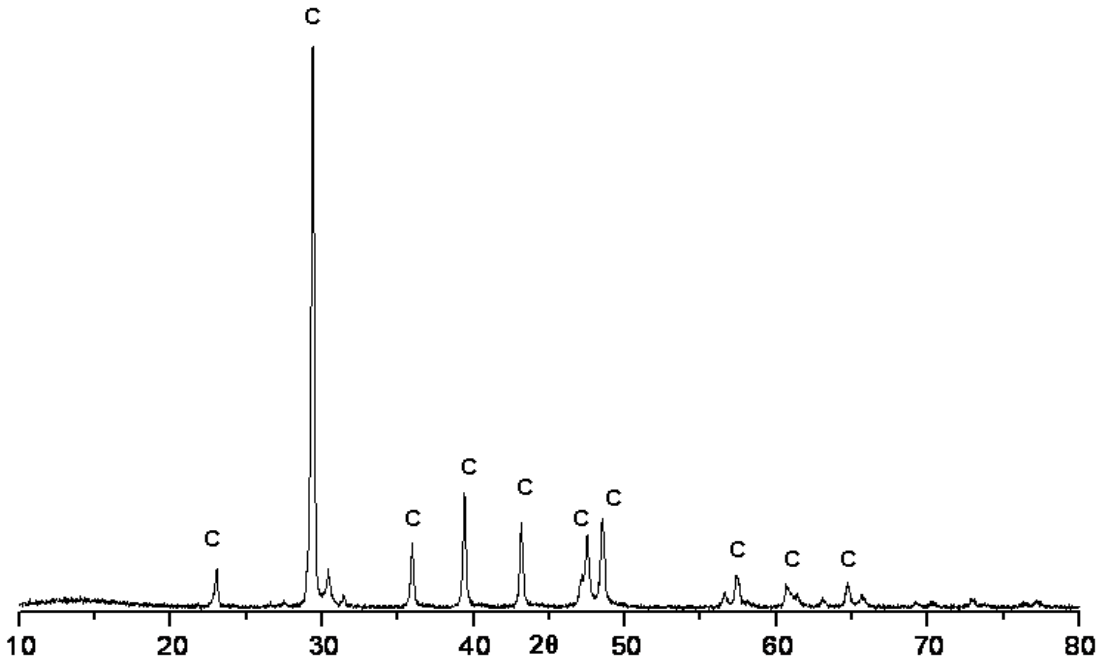

Figure 4. XRD of the carbonated sample (W/L = 0.8) after two curing years (C: Calcite (ICDD 05-0586)).

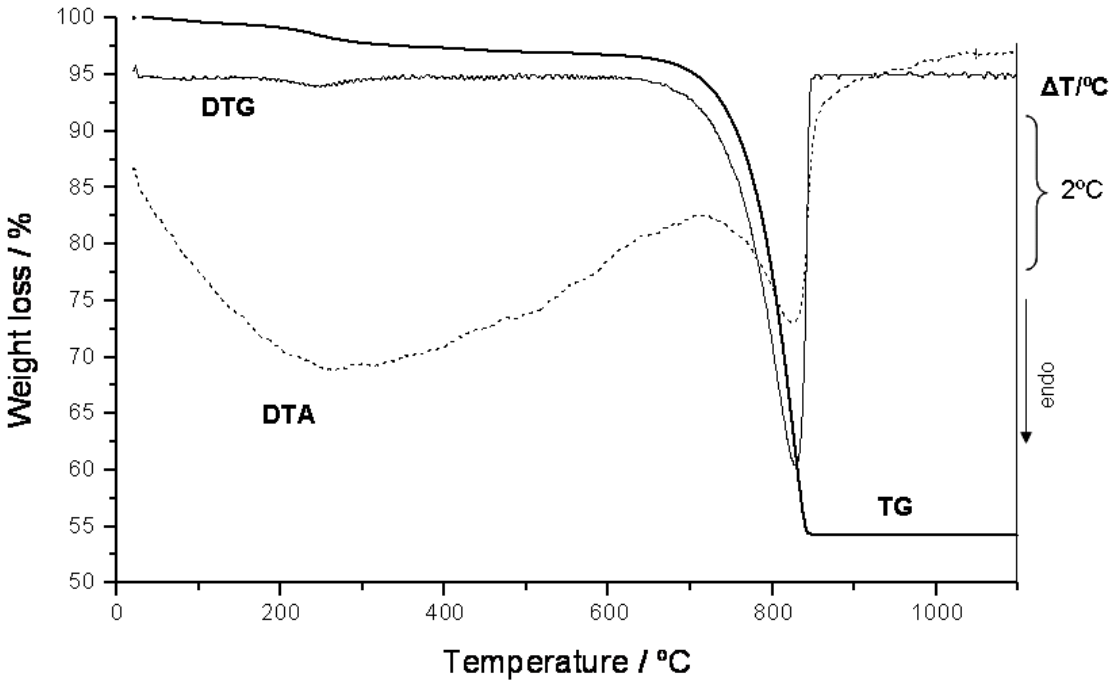

Figure 5. TG, DTG and DTA of the carbonated sample (W/L = 0.8) after two curing years.

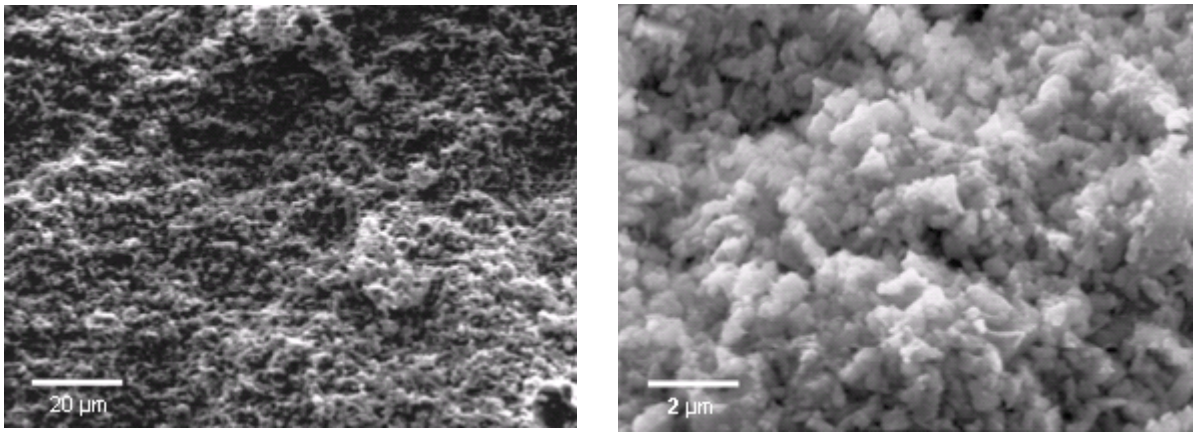

Figure 6. SEM images of carbonated lime pastes at different magnification of the sample (W/L = 1.1) after two curing years.

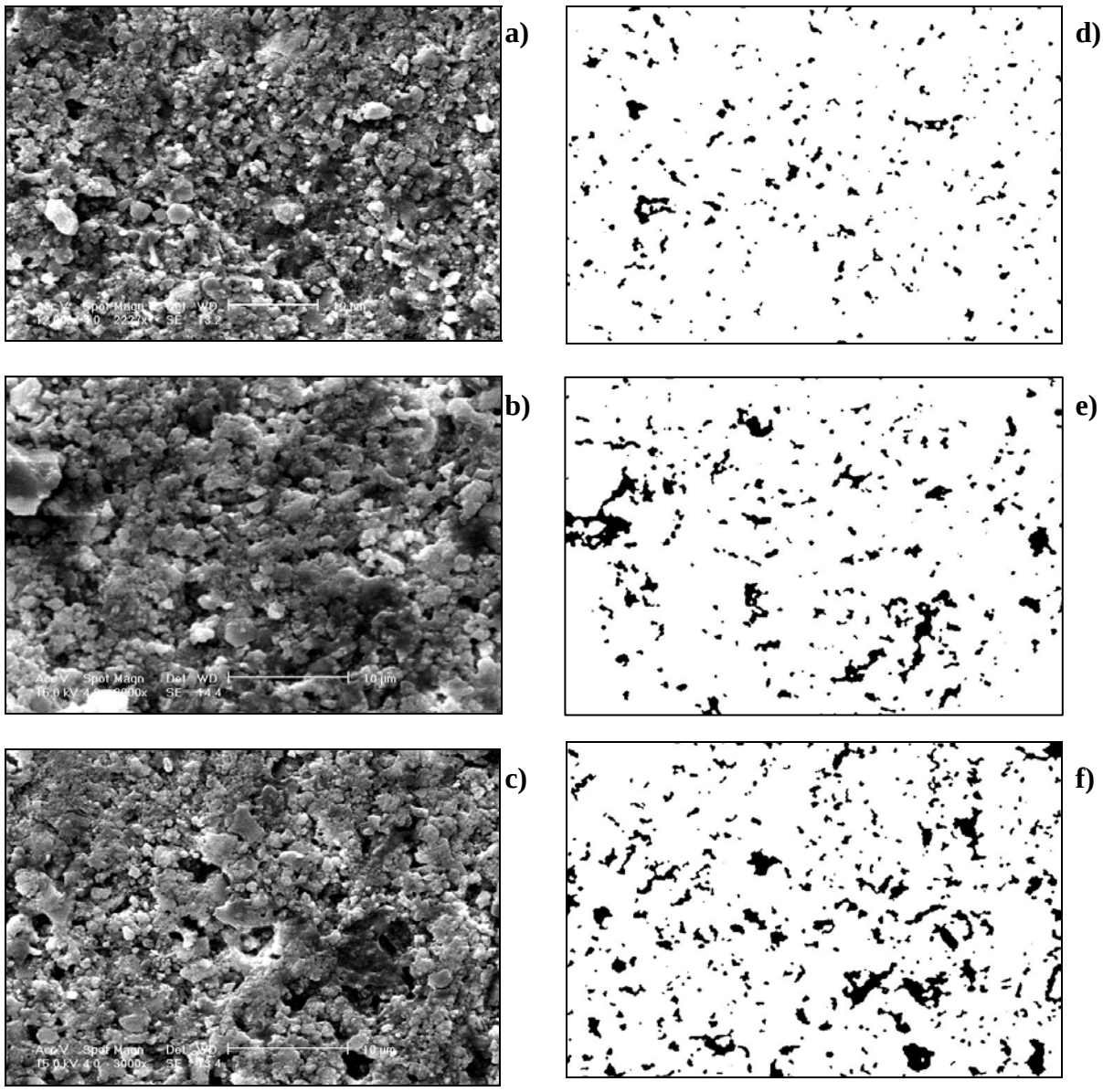

Figure 7. SEM micrographs of a) sample of W/L = 0.8; b) sample of W/L = 1.0; c) sample of W/L = 1.3. Segmented images for DIA analysis: d) sample of W/L = 0.8; e) sample of W/L = 0.8; f) sample of W/L = 0.8.

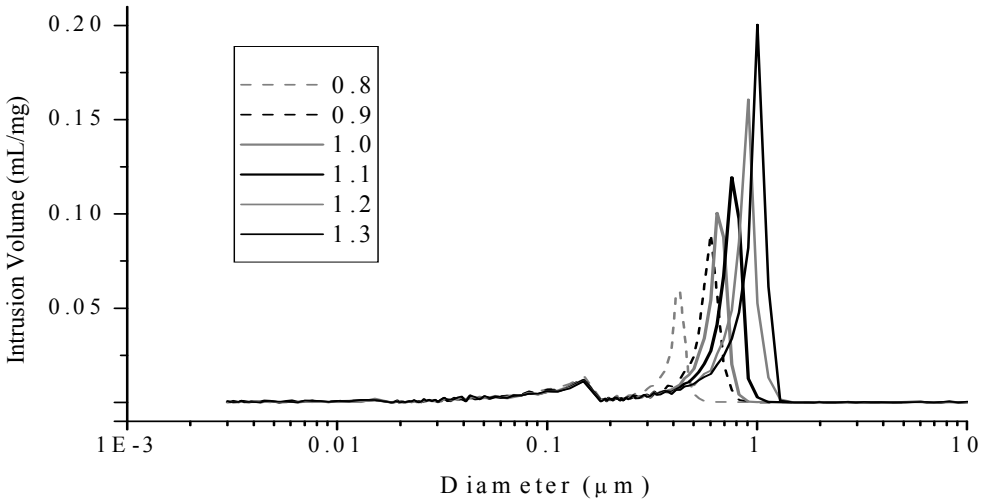

Figure 8. Increment volume intrusion vs. diameter of pore for the six lime pastes.

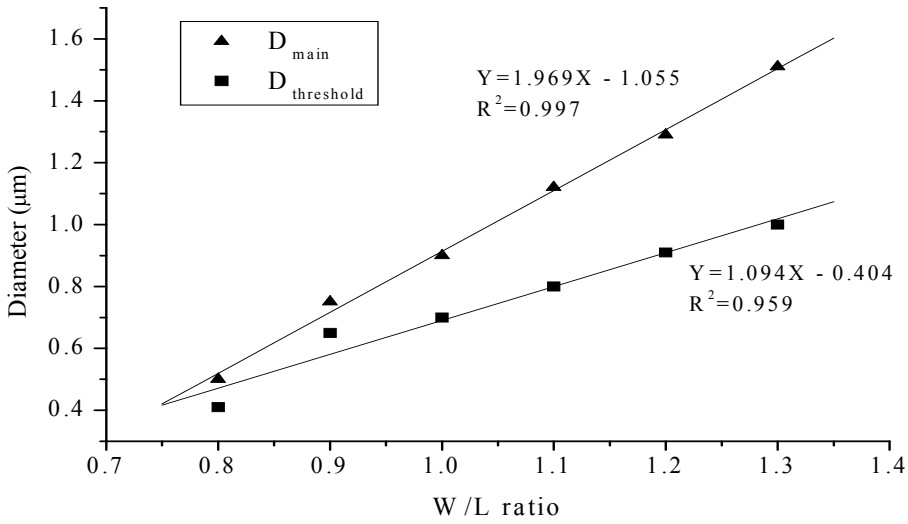

Figure 9. Threshold diameter and the main pore diameter vs. W/L ratio.

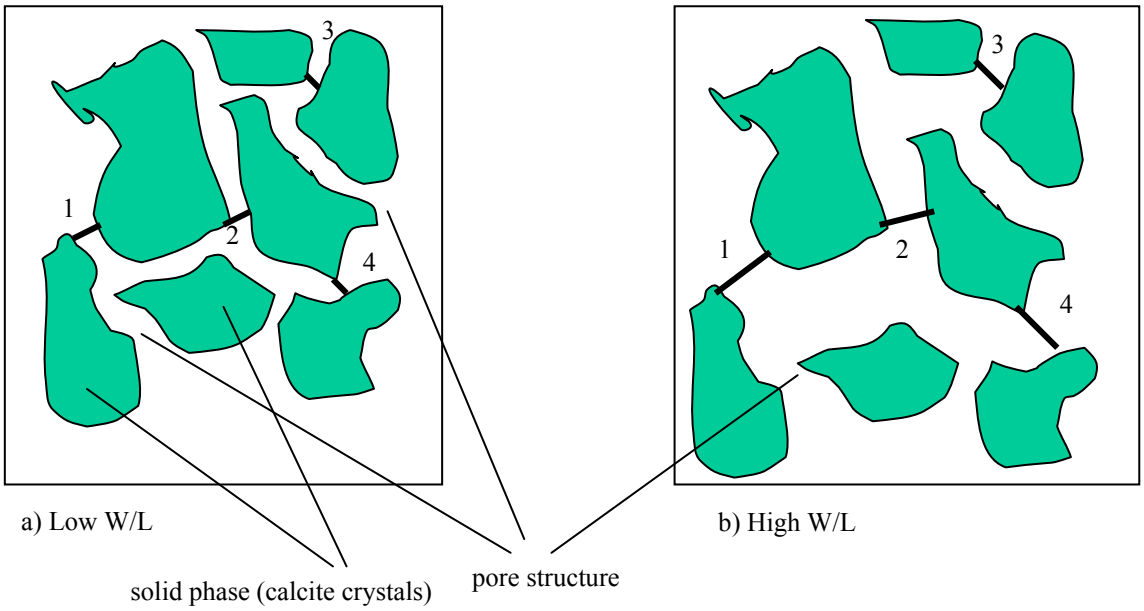

Figure 10. Diagram of the distribution of solid particles in pastes with different W/L ratio, showing a greater distance between solid particles of calcite at the randomly selected four spaces in the highest W/L ratio specimen.

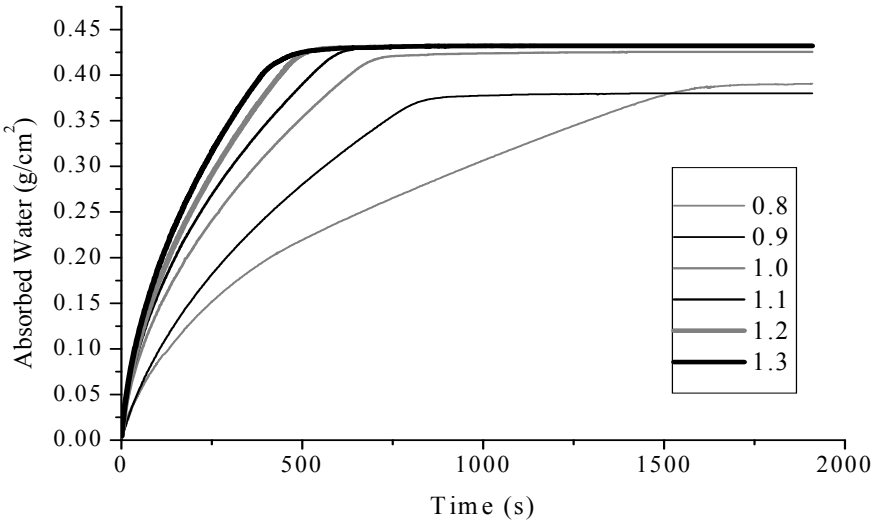

Figure 11. Water absorption vs. time for the different pastes.

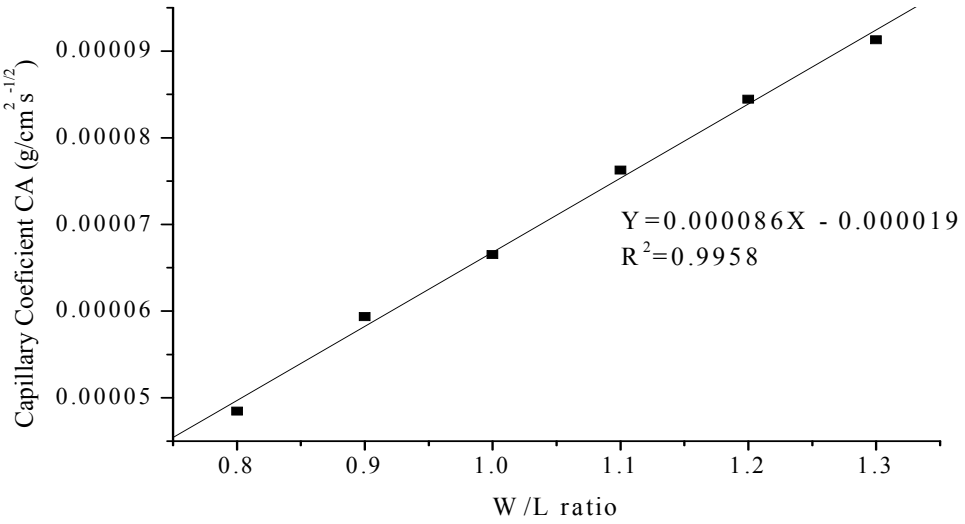

Figure 12. Capillary coefficient for the different lime pastes vs. W/L ratio.

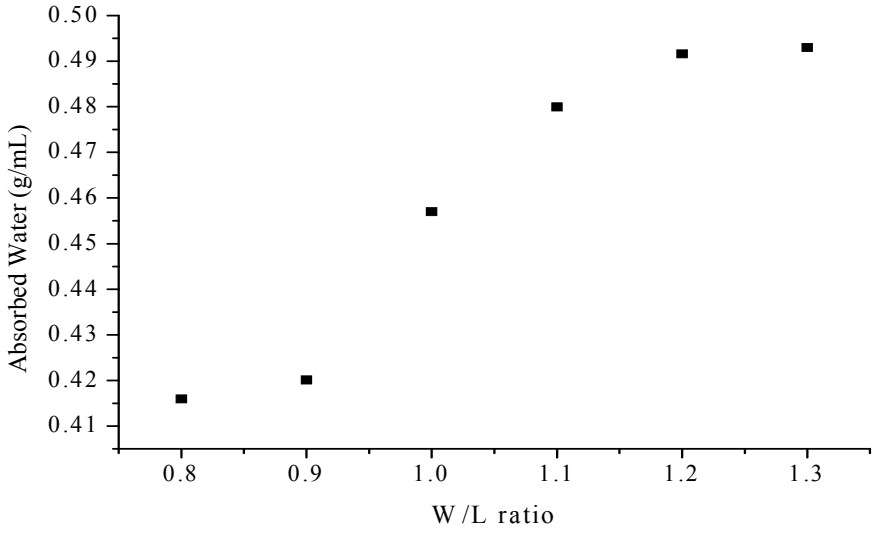

Figure 13. Mass of absorbed water per volume of specimen vs. W/L ratio.

Table 1. Chemical analysis of the main components of the hydrated commercial lime powder (Ecobat®)[a,b].

Lime	I.L.[c] (%)	SiO_2 (%)	CaO (%)	MgO (%)	R_2O_3[d] (%)	SO_3 (%)	Na_2O (%)	K_2O (%)
Ecobat®	25.25	1.03	68.53	3.29	0.89	1.37	0.09	0.05
S.D.	1.20	0.10	1.10	0.42	0.11	0.22	0.02	0.03

[b] The methods specified by the European Standard EN-196 were followed for the chemical analyses.
[c] Ignition loss, indicates the weight loss due to calcinations at 975-1000ºC
[d] Percentage of Fe and Al oxides together.

Table 2. Total porosity for the different lime pastes.

W/L ratio	0.8	0.9	1.0	1.1	1.2	1.3
% P (Hg)	53.7	59.9	58.9	63.0	63.3	66.0
S.D.*	2.4	3.0	1.6	2.8	3.1	2.4
% P (W)	51.8	56.8	56.7	60.1	62.4	62.6
S.D.*	0.1	0.1	0.1	0.5	0.2	0.1

* Standard Deviation

Table 3. DIA results of the pore structure of the different lime pastes.

W/L ratio	0.8	0.9	1.0	1.1	1.2	1.3
Area Fraction (%)	8.0	8.9	9.2	9.8	10.3	11.1
Mean Feret diameter (µm)	0.70	0.76	0.75	0.78	0.82	0.90
Mean shape factor (circularity)	0.76	0.77	0.80	0.83	0.80	0.79

Table 4. Surface fractal dimension (D_S) for the six lime pastes, obtained by MIP and DIA analyses.

W/L ratio	**0.8**	**0.9**	**1.0**	**1.1**	**1.2**	**1.3**
D_S (MIP)	2.373	2.381	2.384	2.391	2.388	2.394
S.D.*	0.011	0.009	0.017	0.005	0.007	0.006
D_S (DIA)	2.340	2.289	2.321	2.265	2.280	2.292
S.D.*	0.021	0.019	0.020	0.009	0.016	0.012

* Standard Deviation